Stem Cell Reports
Report
OPEN ACCESS

Histone H3 Lysine 9 Acetylation Obstructs ATM Activation and Promotes Ionizing Radiation Sensitivity in Normal Stem Cells

Barbara Meyer,[1] Maria Rita Fabbrizi,[1] Suyash Raj,[1] Cheri L. Zobel,[1] Dennis E. Hallahan,[1,2] and Girdhar G. Sharma[1,2,*]

[1]Cancer Biology Division, Department of Radiation Oncology, Washington University School of Medicine, 4511 Forest Park, Saint Louis, MO 63108, USA
[2]Siteman Cancer Center, Washington University School of Medicine, Saint Louis, MO 63108, USA
*Correspondence: sharma@wustl.edu
http://dx.doi.org/10.1016/j.stemcr.2016.11.004

SUMMARY

Dynamic spatiotemporal modification of chromatin around DNA damage is vital for efficient DNA repair. Normal stem cells exhibit an attenuated DNA damage response (DDR), inefficient DNA repair, and high radiosensitivity. The impact of unique chromatin characteristics of stem cells in DDR regulation is not yet recognized. We demonstrate that murine embryonic stem cells (ES) display constitutively elevated acetylation of histone H3 lysine 9 (H3K9ac) and low H3K9 tri-methylation (H3K9me3). DNA damage-induced local deacetylation of H3K9 was abrogated in ES along with the subsequent H3K9me3. Depletion of H3K9ac in ES by suppression of monocytic leukemia zinc finger protein (MOZ) acetyltransferase improved ATM activation, DNA repair, diminished irradiation-induced apoptosis, and enhanced clonogenic survival. Simultaneous suppression of the H3K9 methyltransferase Suv39h1 abrogated the radioprotective effect of MOZ inhibition, suggesting that high H3K9ac promoted by MOZ in ES cells obstructs local upregulation of H3K9me3 and contributes to muted DDR and increased radiosensitivity.

INTRODUCTION

The role of chromatin status on DNA damage response (DDR) and DNA double-strand break (DSB) repair has been extensively investigated in differentiated non-stem and cancer cells. Chromatin structure and remodeling plays an important role in the recruitment/assembly of repair factors and allows their access to DNA lesions (Price and D'Andrea, 2013). Activation of DNA DSB repair machinery is promoted not only by local decondensation of chromatin but also by the binding of heterochromatin-associated proteins and the transient compaction of chromatin (Burgess et al., 2014; Lemaître and Soutoglou, 2014). However, chromatin of differentiated/non-stem and cancer cells is starkly different from the stem/progenitor cells in tissue niches in vivo, such as neural stem cells in the subgranular zone of brain and neural stem cells (NS) cells in culture, intestinal crypt stem cells, testicular stem cells, and embryonic stem cells (ES) in vivo and in culture. These "normal" stem cells are characterized by elevated levels of histone marks associated with active chromatin and lower levels of repressive chromatin (Chen and Dent, 2014). Previously, we have delineated the epigenetic influence of H3K56 acetylation on attenuation of DDR in murine embryonic ES and NS cells, as well as in several tissue niches in vivo, demonstrating H3K56ac as an epigenetic suppressor of DDR that promotes ionizing radiation (IR) hypersensitivity in normal stem cells (Jacobs et al., 2016).

Ataxia telangiectasia mutated (ATM) kinase is involved in multiple DDR processes that include phosphorylation of several histone and non-histone proteins, amplification of the DNA damage signal, repair factor activation, and initiation of the cell-cycle arrest (Shiloh and Ziv, 2013). ATM activation is promoted by its acetylation through Tip60 (Sun et al., 2007). This activation requires the binding of Tip60 to tri-methylated histone H3 lysine 9 (H3K9me3) (Sun et al., 2009), a modification associated with repressive heterochromatin (Grewal and Jia, 2007). H3K9me3 is locally and transiently upregulated around the DNA damage site by the methyltransferase Suv39h1, improving ATM activation via Tip60 (Ayrapetov et al., 2014). Recruitment of Suv39h1 enabling H3K9me3 and assembly of binding partners HP1 and KAP1 is rapid and transient, observed for few minutes after DSB induction. Interestingly, acetylation on the same amino acid residue (H3K9ac) is locally downregulated at the DNA damage sites (Bártová et al., 2011).

We compared karyotypically normal, early-passage, radiosensitive murine ES and NS with the isogenic radioresistant non-stem cells (ED and ND), proliferating at identical rates in culture; to investigate the differential regulation of DNA damage and apoptotic responses of radiosensitive stem and radioresistant non-stem cells (Jacobs et al., 2016). In this study, we demonstrate constitutively high H3K9ac but low H3K9me3 levels in ES that fails to downregulate H3K9ac at the DSB sites (microirradiation tracks), unlike the ED. Suppression of the H3K9 acetyltransferase monocytic leukemia zinc finger protein (MOZ) reduced H3K9ac in ES, protected them from IR-induced apoptosis, and improved ES survival after irradiation. On the contrary, knockdown of MOZ did not protect

non-stem or cancer cells from IR-induced cell death. Besides ES, reduction of IR-induced apoptosis after MOZ knockdown in human neuroprogenitor cells suggests that a transient suppression of MOZ may very likely be a useful therapeutic strategy for radioprotection of human neuroprogenitor cells.

RESULTS

Embryonic and Neural Stem Cells Exhibit High H3K9 Acetylation and Low H3K9 Tri-methylation In Vivo and In Vitro

We investigated the H3K9 modifications in embryonic and adult stem cell populations and found that the inner cell mass of the mouse blastocyst (embryonic day 4.5 [E4.5], wild-type C57BL/6) containing the pluripotent ES cells showed markedly high H3K9 acetylation compared with the trophoblast cells (Figure 1A). The basal expression of histone H3 was similar between the two cell types (Figure 1A). ES cells in culture were co-plated with isogenic non-stem ED cells before fixation as described previously (Jacobs et al., 2016). H3K9ac was detected with the stem cell-specific transcription factor SOX2. SOX2-positive cells showed significantly elevated H3K9ac compared with the SOX2-negative ED cells (Figure 1B); however, H3K9me3 was diminished in stem cells in contrast to the non-stem cells (Figure 1B). Although differentiation procedures yield highly enriched non-stem cells in culture, directly derived cells (ED) often retain a minimal SOX expression, probably due to its role in cell fate determination (Robles et al., 2011). Immunoblotting also corroborated high H3K9ac in ES compared with ED (Figure 1C). NS cells, isolated from newborn mouse hippocampi compared with their non-stem cell (ND) counterparts, were also investigated (Jacobs et al., 2016). Immunoblotting revealed high H3K9ac in NS compared with SOX2-negative ND (Figure 1D). To confirm this, we investigated adult NS cells in the dentate gyrus niche of mouse brain. SOX2-positive adult NS/neuroprogenitor cells also displayed high H3K9ac, but reduced H3K9me3 compared with surrounding non-stem cells in the tissue niche (Figure 1E). Similar status was observed in spermatogonial stem cells (Figures S1A and S1B) in mouse testis, suggesting similar H3K9 modifications in several stem cell types. Some PLZF negative non-stem cells (mostly spermatids) also displayed higher H3K9 acetylation, likely due the role in the histone-protamine exchange (Song et al., 2011). Together, these results indicate that H3K9 is differentially modified in murine ES and neuroprogenitor and spermatogonial stem cells, displaying high acetylation (H3K9ac) but low tri-methylation (H3K9me3).

Embryonic Stem Cells Fail to Efficiently Downregulate H3K9 Acetylation and Upregulate H3K9 Methylation at the DNA Breaks

H3K9ac has been shown to be downregulated locally around the DNA damage sites in a fraction of murine ES cells (Bártová et al., 2011). We tested whether in ES such downregulation occurs around DSB sites despite the significantly high global H3K9 acetylation in contrast to the ED. We co-plated ES and ED and irradiated ES in close proximity of ED using laser microirradiation. Induction of DSBs along the microirradiation track was visualized by labeling the DSB marker γH2AX together with staining for H3K9ac while ES were identified by SOX2-positive staining (Figure 2A). Figure S2A shows a representative example of an uncropped image of co-plated ESCs and EDCs in same line of microirradiation. Most of the ED cells showed depleted H3K9ac at the DSB track, quantified in the fluorescent signal-intensity line profile across the irradiated nuclei (Figure 2A, upper panel), which does not occur due to eviction of H3 from the damaged sites (Jacobs et al., 2016). But unlike ED, ES cells did not downregulate H3K9ac at the DNA DSBs with same proficiency as observed in ED (Figure 2A, lower panel). ES displayed significantly reduced and very diffused, if any, γH2AX signal at DNA lesions compared with ED, which is very likely due to reduced ATM activation that has been previously shown in stem cells (Jacobs et al., 2016). Unirradiated ES (Figure S2D) and ED (Figure S2E) displayed uneven H3K9ac profiles throughout the nuclei. Within the DNA damage sites, in and along the track, ED showed clearly reduced H3K9ac at all points of the intensity profile (Figure S2C), while in ES H3K9ac remained high (Figure S2B) and comparable with that in unirradiated cells. We quantified the number of ES and ED cells that showed clear downregulation of H3K9ac at DSBs and found that about 90% of ED locally deacetylated H3K9, while only 40% of analyzed ES showed depletion of H3K9ac (Figure S2F). These results suggest that H3K9 acetylation and local H3K9 deacetylation in response to DNA damage induction are differentially regulated in stem compared with non-stem cells.

H3K9me3 is locally and transiently upregulated around the DNA damage site by histone methyltransferase Suv39h1, promoting ATM activation via Tip60 (Ayrapetov et al., 2014). We tested whether such upregulation occurs in ES cells. While ED showed a detectable increase in H3K9me on the DSB tracks (Figure 2B, upper panel), ES often failed to upregulate H3K9me3 at the tracks (Figure 2B, lower panel). Quantification of the number of cells with upregulated H3K9me3 at DSBs revealed about 90% of ED with H3K9me3-positive tracks, while only 5% of analyzed ES showed a local increase of H3K9me3. This H3K9 epigenetic modification is quick and transient, with the highest

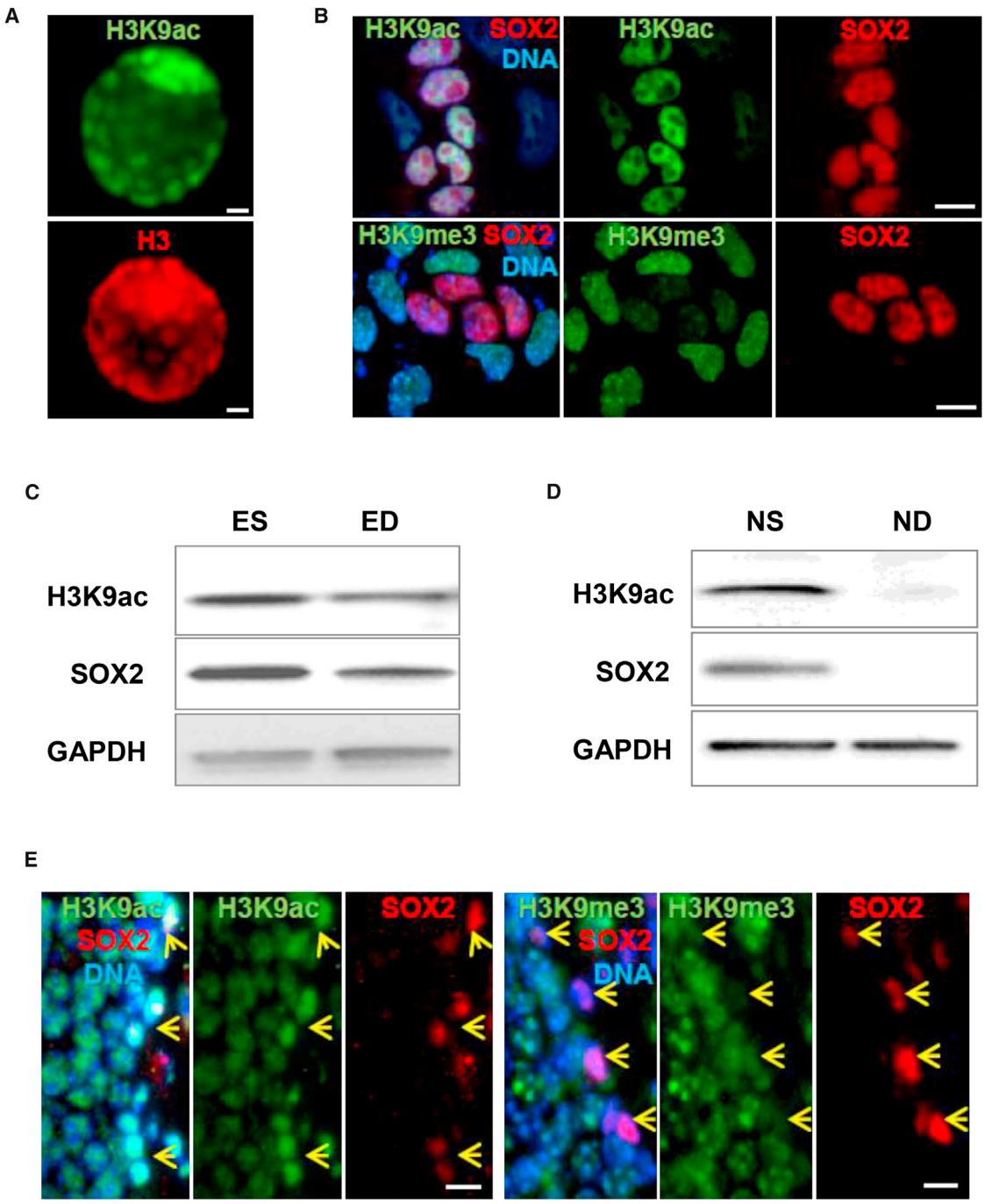

Figure 1. Embryonic Stem and Neural Progenitor Cells Exhibit High H3K9 Acetylation and Low H3K9 Tri-methylation In Vitro and In Vivo

(A) Mouse blastocysts (E4.5) fixed and stained for H3K9ac or H3.

(B) H3K9ac (upper panel) or H3K9me3 (lower panel) with SOX2 detected in co-cultures of ESCs and EDCs. DNA labeled with DAPI.

(C) H3K9ac, SOX2, and GAPDH detected in lysates of ES and ED using immunoblot.

(D) H3K9ac, SOX2, and GAPDH detected in NS and ND lysates using immunoblot.

(E) Tissue sections of the dentate gyrus in hippocampus obtained from brains of WT C57BL/6 mice and H3K9ac (left panels) or H3K9me3 (right panels) stained with SOX2 and DNA labeled with DAPI. Arrows indicate SOX2-positive stem and progenitor cells with high H3K9ac and low H3K9me3 levels.

Scale bars, 10 μm.

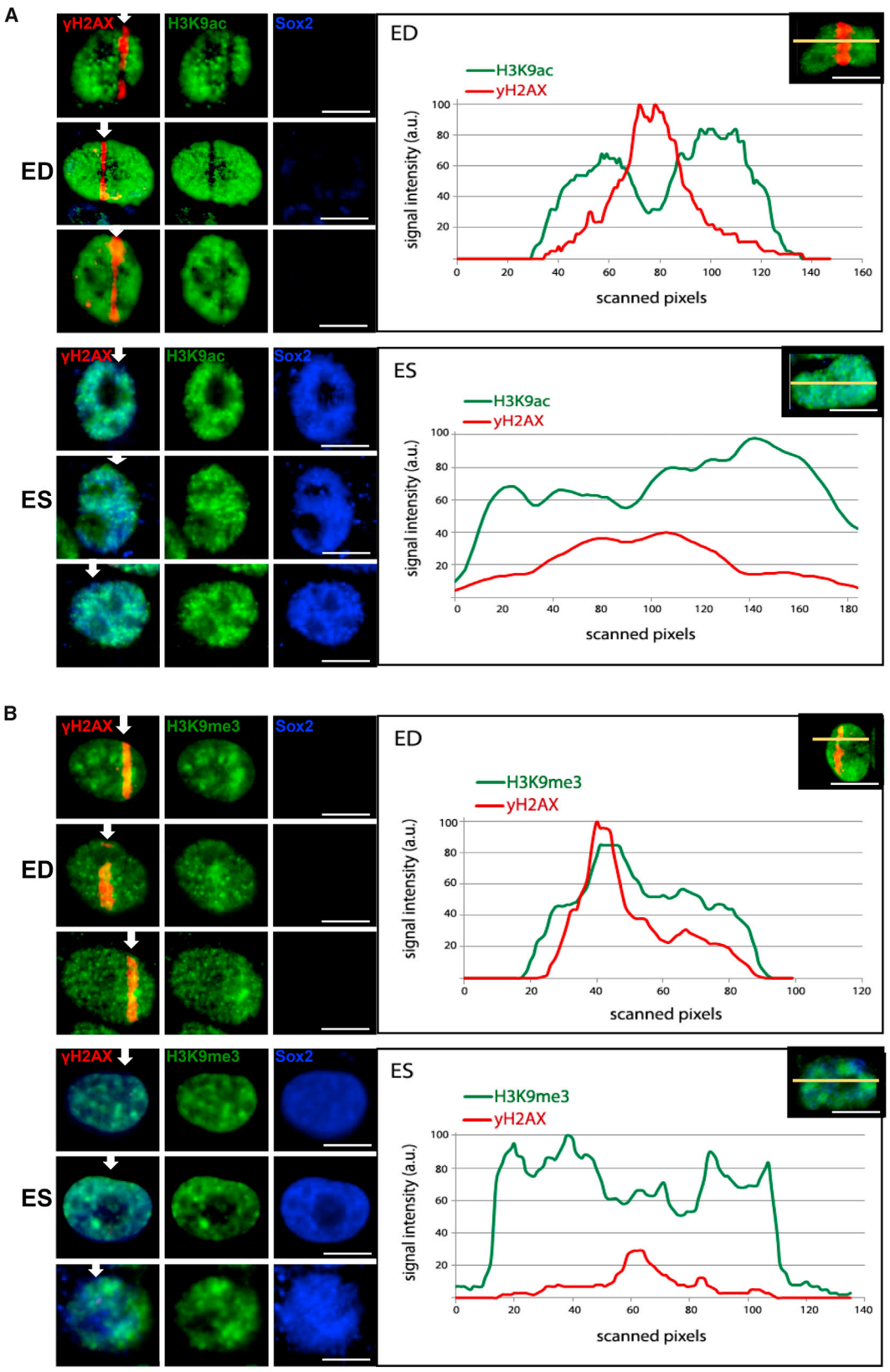
A
γH2AX
H3K9ac
Sox2
ED
H3K9ac
γH2AX
signal intensity (a.u.)
scanned pixels
ES
B
H3K9me3
(legend on next page)

methylation tracks observed within 2 min of irradiation (Figure S2F). These results establish differential regulation of these epigenetic modifications at or around DNA damage sites in stem cells.

Downregulation of MOZ Reduced H3K9 Acetylation and Improved DNA Damage-Induced Activation of ATM and DNA Repair Efficiency in ES cells

While the precise role of H3K9 deacetylation at DSBs has not been identified as yet, the upregulation of tri-methylation at the same amino acid residue around the DSBs via Suv39h1 has been explicitly shown to be required for the activation of ATM through Tip60 (Ayrapetov et al., 2014). We therefore tested the hypothesis that inefficient H3K9 deacetylation at DNA break site hinders the local upregulation of H3K9me3 and thereby contributes to the reduced ATM activation as observed in stem cells. We investigated whether ATM activation could be promoted/restored in stem cells by downregulation of H3K9ac. Transient knockdown of the acetyltransferase MOZ resulted in a reduction of H3K9ac in stem cells (Figure 3A), while overexpression of deacetylase SIRT6 (Figure S3A) or inhibition of acetyltransferase GCN5 (Figure S3B, left) did not influence H3K9ac levels. Besides, knockdown of GCN5 did not reduce IR-induced apoptosis (Figure S3B, right). Furthermore, a faster and longer activation of ATM (phospho-serine 1981) was observed when MOZ expression was inhibited (Figure 3B). Detection of phospho-ATM with flow cytometry corroborated improved ATM activation with MOZ inhibition (Figure 3C). Total ATM protein levels are similar in ESCs and EDCs (Jacobs et al., 2016). We measured the kinetics of DSB repair after MOZ depletion by comet assay and observed an improvement in DNA repair in stem cells treated with MOZ small interfering RNA (siRNA) (Figure 3E), almost comparable with the DSB repair in irradiated ED without MOZ inhibition. MOZ inhibition in ED had no effect (Figure 3E). The cell-cycling rates of both ES and ED have been shown previously to be identical (Jacobs et al., 2016). Analysis of chromosomal aberrations also revealed an improved repair and reduced residual chromosome and chromatid breaks in MOZ-depleted stem cells after irradiation (Figure 3D). These results suggest that MOZ activity in ES cells antagonizes or interferes with full activation of ATM in response to DNA damage, potentially by sustained maintenance of elevated H3K9ac levels and thereby inhibiting tri-methylation of H3K9. We also observed increased activation of ATM after MOZ suppression to be dependent upon the H3K9 methyltransferase Suv39h1 (Figure 3F). Endogenous SIRT1 (Figure S3C) or SIRT6 (Figure S3D) recruitment could not be detected in ES or ED cells using microirradiation. However, it has previously been shown that SIRT1 is redistributed to the DNA damage in murine ES cells (Oberdoerffer et al., 2008). Using a SIRT6-GFP overexpression approach, we were able to detect rapid recruitment in ED but not in ES (Figure S3E). Instead there was no recovery of the bleached GFP, suggesting a stable binding of SIRT6 to the chromatin in ES cells. Whether this is influenced by MOZ or an independent mechanism contributing to inefficient H3K9 deacetylation requires further investigation.

Suppression of H3K9 Acetyltransferase MOZ Reduced IR Sensitivity of Stem Cells

Improvement of DSB repair in stem cells has a potential for development of stem cell-specific radioprotectors. We therefore investigated whether the knockdown of MOZ was effective in improving the overall survival of ES cells after irradiation. Significantly decreased IR-induced apoptosis was observed in ES with depletion of MOZ (Figure 4A), while upregulation of SIRT6 had no influence on apoptosis (Figure S4A). Besides the ES used throughout this study (LK-1), an additional ES cell line, EDJ22, also showed similar radioprotection with the MOZ knockdown (Figure 4B). However, LK-1-derived non-stem ED cells were not protected (Figure 4C), with downregulation of MOZ expression (Figure 4D). In addition, medulloblastoma Daoy HTB-186 cells (Figure S4B) and glioma GL261 cancer cells (Figure S4C) were also not radioprotected after MOZ suppression. Clonogenic survival and radiosensitivity of ES cells improved with MOZ downregulation (Figure 4E). Interestingly, simultaneous downregulation of MOZ and ATM reduced DSB repair efficiency, confirming

Figure 2. Embryonic Stem Cells Fail to Downregulate H3K9 Acetylation and Upregulate H3K9 Methylation Locally at DNA Damage Sites Compared with Differentiated Cells

ES were co-plated with isogenic non-stem ED cells. Cells were microirradiated subnuclearly in a line across the ES and ED in same region of interest (ROI) crossing through both cell types.

(A) ED and ES microirradiated and fixed immediately after irradiation and H3K9ac and γH2AX detected along with Sox2 (arrow indicates laser ROI). Quantification of fluorescence intensities along the yellow line is depicted in the corresponding graph on the right. ED are shown in the top panel and ES adjacent to ED in the line of irradiation, treated in the same way, in the lower panel.

(B) ED and ES microirradiated and fixed immediately after irradiation and H3K9me3 and γH2AX detected along with Sox2. Fluorescence intensities along the yellow line is depicted in the corresponding graph on the right. ED are shown in the top panel and ES adjacent to ED in the line of irradiation, treated in the same way, in the lower panel.

Scale bars, 10 μm.

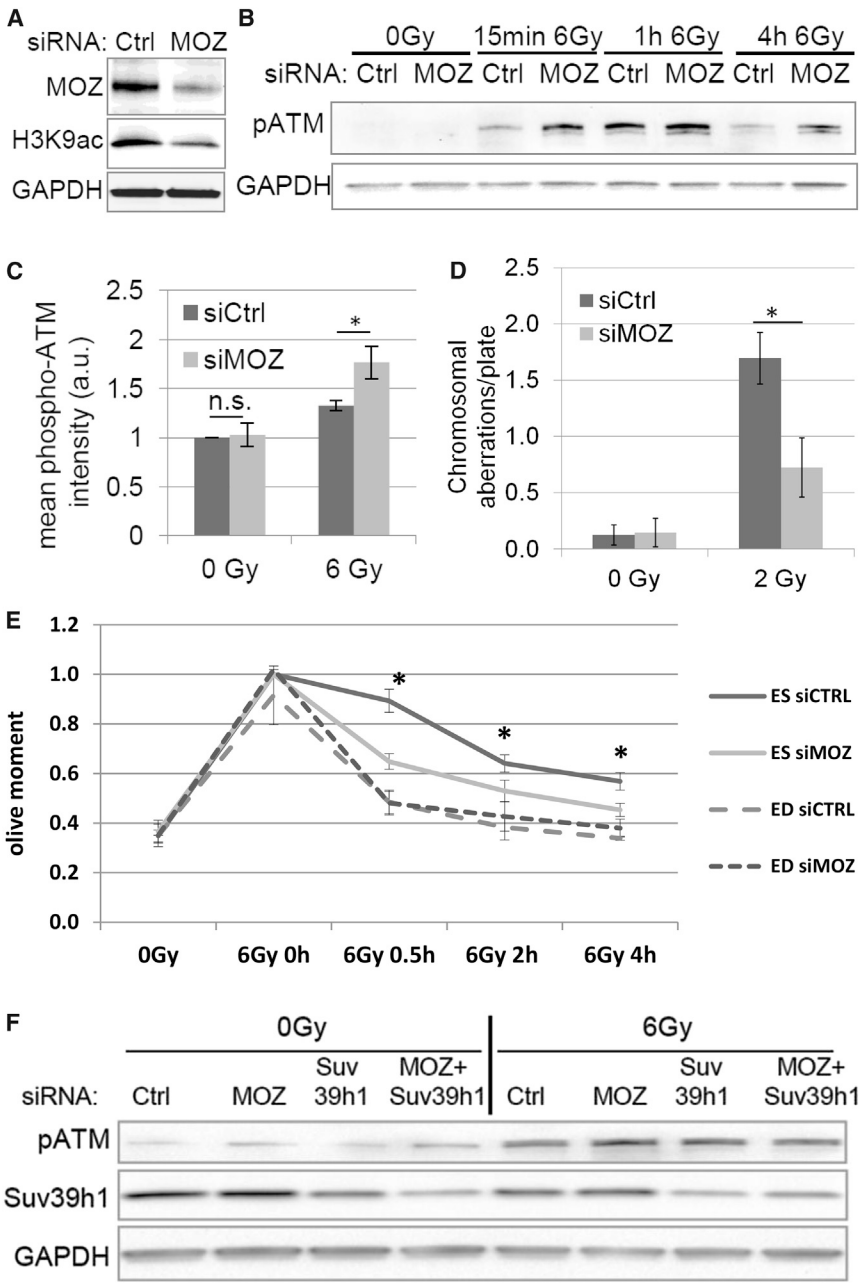

Figure 3. Suppression of MOZ Decreases H3K9 Acetylation and Improves ATM Activation and DNA Repair Efficiency

ES cells were treated with control siRNA (siCtrl) or MOZ siRNA (siMOZ).

(A) MOZ, H3K9ac, and GAPDH detected in cell lysates using immunoblot.

(B) pATM (phospho-S1981) and GAPDH detected using immunoblot after 6 Gy irradiation at indicated time points.

(C) pATM (phospho-S1981) analyzed with flow cytometry 30 min after 6 Gy irradiation. Values were normalized to the 0-Gy siCtrl sample. Three independent experiments were performed.

(D) Chromosomal aberrations per metaphase plate quantified at 7 hr after 2 Gy irradiation. Three independent experiments were performed.

(E) ES and ED treated with siCtrl or MOZ siRNA were analyzed by comet assay. Values were normalized to the 0-Gy time point. Three independent experiments were performed.

(F) ES cells treated with control, MOZ, Suv39h1, or both MOZ and Suv39h1 siRNA and pATM (phospho-S1981), Suv39h1, and GAPDH detected by immunoblot in lysates 30 min after 6 Gy irradiation.

Error bars denote SD. *$p < 0.05$; n.s., not significant ($p > 0.05$).

that improvement in radiosensitivity of stem cells by MOZ inhibition is largely through ATM activation, as ATM inhibition reverses the MOZ inhibition-driven improvement in DSB repair and IR sensitivity phenotype (Figure 4F). MOZ HAT$^{-/-}$ hematopoietic and neural progenitors show a higher expression of p16 leading to senescence (Perez-Campo et al., 2014), and MOZ has been shown to inhibit the p16 pathway in mouse embryonic fibroblasts (MEFs) (Sheikh et al., 2015a). Interestingly, we observed no effect on p16 levels with the MOZ knockdown (Figure S4D), indicating that the analyzed cells were not senescent. It has previously been shown that restoration of the abrogated G1 checkpoint in murine ESCs can reduce their radiosensitivity (Hong and Stambrook, 2004). We observed that despite MOZ knockdown and improved ATM activation, ESCs fail to arrest in G1 (Figure S4E), suggesting that the radioprotection by MOZ suppression is mediated by an improved DNA repair rather than by checkpoint activation. The IR-induced apoptosis of ES cells was reduced by MOZ knockdown only if Suv39h1 was normally expressed, while simultaneous downregulation of MOZ and Suv39h1 did not protect stem cells from apoptosis (Figure 4G). The

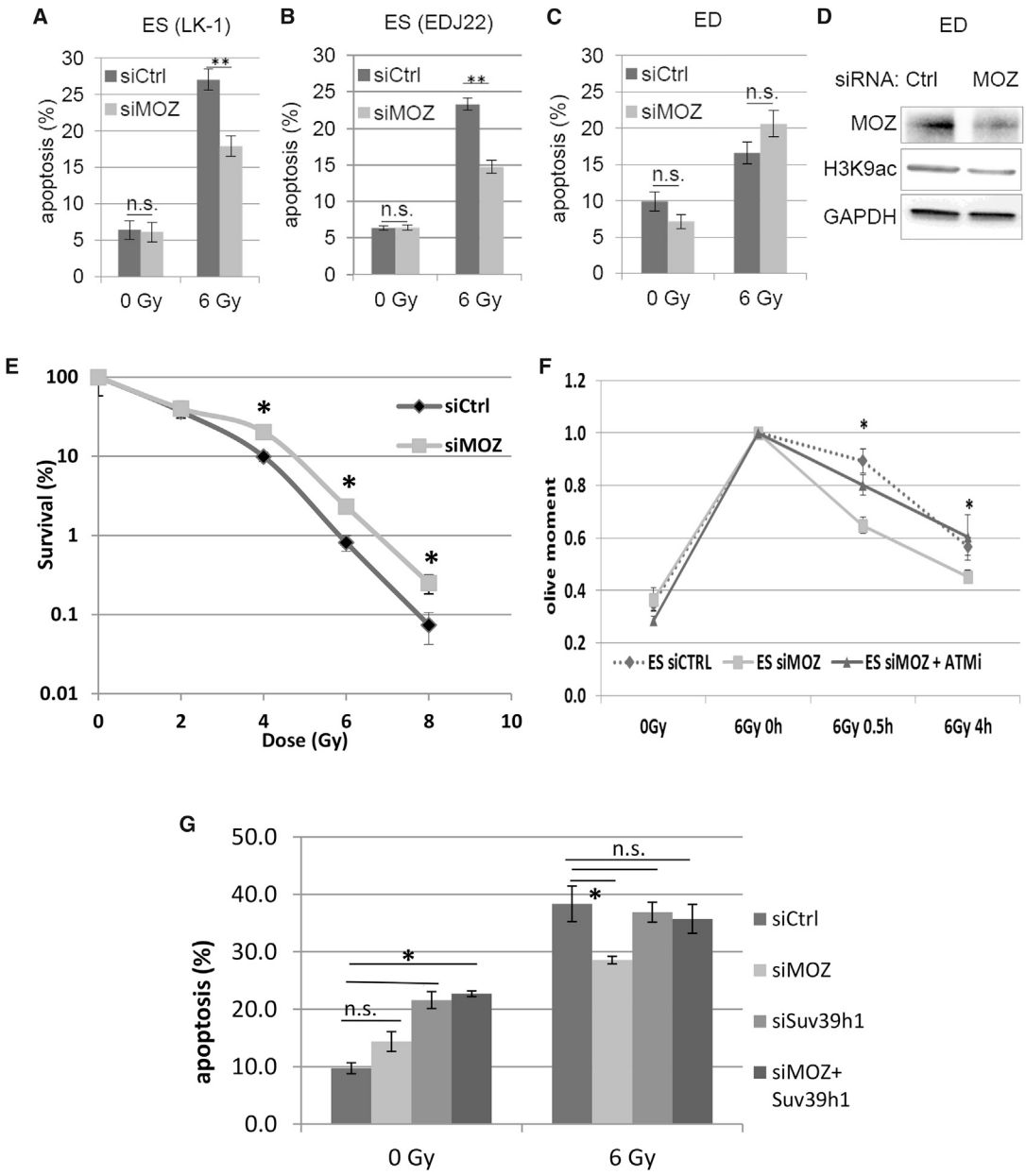

Figure 4. Downregulation of MOZ Expression Diminished Radiation-Induced Apoptosis in a Suv39h1-Dependent Manner and Increased Survival in Embryonic Stem Cells

Cells were treated with control siRNA (siCtrl) or MOZ siRNA (siMOZ).

(A) ES cell line LK-1 irradiated with 6 Gy and apoptosis analyzed after 16 hr by annexin V labeling. Three independent experiments were performed.

(B) As a comparison, ES line EDJ22 was used only in this experiment and analyzed as in (A). Three independent experiments were performed.

(C) ED cells analyzed as in (A). Three independent experiments were performed.

(D) MOZ, H3K9ac, and GAPDH detected in ED lysates by immunoblot.

(E) Clonogenic survival of ESCs analyzed after indicated doses of irradiation. Three independent experiments were performed.

(F) ES treated with siCtrl, MOZ siRNA, or MOZ siRNA with ATM inhibitor analyzed by comet assay. Values were normalized to the 6-Gy time point. Three independent experiments were performed.

(G) ES treated with control, MOZ, Suv39h1, or both MOZ and Suv39h1 siRNA and analyzed as in (A). Three independent experiments were performed.

Error bars denote SD. *$p < 0.05$, **$p < 0.01$; n.s., not significant ($p > 0.05$).

higher apoptosis rate in the 0-Gy control after inhibition of Suv39h1 alone or in combination with MOZ can likely be due to the cells' inability to recruit ATM and HP1 to repair DNA damage at the basal level. To confirm the significance of these observations made in murine stem cells, we then analyzed neuroprogenitor cells directly derived from human ESCs. The differentiation was visible in cell morphology (Figure S4F) and confirmed by OCT4 and SOX1 detection (Figure S4G). Human neuroprogenitors were also radioprotected by MOZ knockdown (Figure S4H), corroborating our findings in murine ESCs. Together, these observations indicate a significant role of MOZ in the radiation response of stem cells, suggesting that transient suppression of MOZ can potentially be a useful therapeutic strategy to prevent IR-induced stem cell death.

DISCUSSION

The repair of DNA damage requires dynamic chromatin alterations comprising both transient decondensation and compaction of chromatin locally around the DSB sites. Stem cells display a uniquely open, undefined chromatin structure, but our understanding of its consequences in activation of DDR and recruitment of DNA repair factors is still very limited. In this study, we describe that the inhibition of acetyltransferase MOZ reduces H3K9 acetylation and promotes the activation of ATM via the histone methyltransferase Suv39h1, leading to an increase in DNA repair efficiency and decreased IR-induced cell death.

H3K9 modifications have been previously analyzed in ESCs (Lee et al., 2004; Meshorer et al., 2006; Azuara et al., 2006; Loh et al., 2007). This study supports previous observations and additionally demonstrates an increased constitutive H3K9ac along with distinctly reduced H3K9me3 in stem cells, in contrast to the isogenic non-stem ED cells in culture as well as in vivo. Local downregulation of H3K9ac has been reported in ESCs, accompanying recruitment of the transcription factor OCT4 to DNA lesions (Bártová et al., 2011). In the same study, a downregulation of H3K9 acetylation was not observed in one-third of the analyzed stem cells, which is in agreement with our finding of a local decrease of H3K9ac in 40% of the stem cells in culture. Moreover, our work compares the local H3K9 deacetylation at or around DSBs in ES directly with the frequency of H3K9ac downregulation in non-stem ED cells, showing a less efficient deacetylation response in ES cells. While the function of the local H3K9ac downregulation in the DDR is not clear, the regulation of ATM activation by H3K9me3 through Suv39h1 has been extensively studied (Ayrapetov et al., 2014; Sun et al., 2009). We hypothesize that deacetylation at H3K9 is a prerequisite to allow tri-methylation at this same amino acid residue for efficient ATM activation. In accordance, we observed that while ED cells show an increase in H3K9me3 at the DSB tracks, ES did not display such chromatin modification. The lower percentage of ED positive for H3K9me3 compared with deacetylated H3K9 can be explained by the very transient/temporal nature of the process: in fact we observed that the high percentage of ED showing tri-methylation can be observed only within 2 min after the DNA damage induction, and this percentage reduced drastically at 10 min after DSB induction. We thus provide evidence that differential ATM activation through Suv39h1 is influenced by the characteristic chromatin profiles. Suppression of Suv39h1 methyltransferase alone had a limited effect on ATM activation or IR-induced apoptosis of stem cells. This is in accord with our hypothesis that H3K9 deacetylation is required before Suv39h1-mediated methylation of H3K9, and therefore Suv39h1 activity is restricted in stem cells with consistently elevated H3K9ac.

MOZ regulates H3K9ac at Hox gene promoters, but no global downregulation of H3K9ac was detected in $MOZ^{+/-}$ or $MOZ^{-/-}$ embryos compared with WT mice (Voss et al., 2009). However, with a transient MOZ knockdown approach, we were able to observe a global downregulation of H3K9ac. It is very likely that prolonged absence of functional MOZ could partly be compensated by the activity of other redundant H3K9 acetyltransferases such as GCN5 in $MOZ^{-/-}$ cells. However, we cannot exclude that MOZ has a broader effect on global H3K9 acetylation only in specific types of embryonic or adult stem/progenitor cells.

In this study, transient MOZ suppression did not alter p16 expression. MOZ is important for suppression of p16 that is required to maintain self-renewal capacity, and MOZ $HAT^{-/-}$ hematopoietic cells and NSCs show enhanced $p16^{INK4A}$ expression and an early replicative senescence (Perez-Campo et al., 2014). Similarly, in MEFs MOZ functions as an inhibitor of senescence via the INK4A-ARF pathway, with $MOZ^{-/-}$ MEFs showing a reduction in proliferation only at late passages and no increased levels of apoptosis (Sheikh et al., 2015a). This suggests that only prolonged absence of MOZ leads to cellular senescence, in agreement with our finding that the transient MOZ suppression did not alter p16 expression.

We propose that transient inhibition of MOZ could be beneficial in stem cell survival by improved ATM activation and DNA repair, with a negligible effect on differentiated non-stem or cancer cells. Elevated global H3K9ac, like H3K56ac, is essential for stem cell-specific transcriptome and has possibly other crucial diverse functions in stem cells. Therefore, a total knockout of MOZ from stem cells, or prolonged depletion, would be detrimental for "stemness" state, and also in non-stem cells because of likely induction of senescence in both cell types and lack of DNA

damage-induced G1 checkpoint arrest in differentiated cells. It has been suggested that MOZ promotes induction of the G1 cell-cycle arrest in MEF cells through its interaction with p53, improving cellular viability (Rokudai et al., 2009).

Suppression of MOZ protected a fraction of cells from IR-induced apoptosis, increased DNA repair proficiency, and improved survival by a factor of 2 to 3 between 4 and 8 Gy. This also warrants that MOZ is not the sole epigenetic/molecular regulator decisive of the stem cell radiation response. We have recently established that ES and NS cells can be radioprotected by transiently diminishing H3K56ac (Jacobs et al., 2016), which is also characteristically high in stem cells. Besides, we have identified stem cell-specific differential signaling regulation by protein phosphatase PP2A (M.R.F. et al., unpublished data) that contributes to stem cell IR hypersensitivity. We have thus elucidated epigenetic and molecular signaling rheostats that pluralistically regulate and collectively promote IR hypersensitivity of stem cells. Interestingly, use of MOZ inhibition has been suggested earlier for the treatment of certain types of lymphoma and leukemia (Sheikh et al., 2015b) as well as for a potential induction of senescence in cancer stem cells (Perez-Campo et al., 2014). The expression of mutated MOZ has been associated with the formation of medulloblastoma (Wu et al., 2012). We observed that medulloblastoma cells undergo increased apoptosis when MOZ was suppressed, which supports the notion that inhibition of MOZ could have a radiosensitizing effect in certain cancer types but be radioprotective to normal stem cells.

However, development of a pharmacological transient inhibitor of MOZ would be essential to analyze the therapeutic potential of MOZ inhibition on radioprotection in mouse preclinical models. This study proposes MOZ histone acetyltransferase as a promising target for development of radioprotective agent.

EXPERIMENTAL PROCEDURES

RNA Interference

siRNA against MOZ, GCN5, and Suv39h1 was used at 50 nM for 24 hr. See Supplemental Experimental Procedures for a detailed description.

X-Ray Irradiation and Microirradiation

Cells were irradiated with 160 keV X-rays with indicated doses at a dose rate of 1.7 Gy/min. For microirradiation, co-plated embryonic and differentiated cells were cultured for 2 days in 70 μM bromodeoxyuridine and irradiated with a 405- and 633-nm laser. See Supplemental Experimental Procedures for further details.

Apoptosis Assay

Cells were trypsinized at indicated time points after irradiation and labeled using the FITC Annexin V Apoptosis Detection Kit I (BD Pharmingen) according to the manufacturer's instructions. At least 5,000 cells were analyzed by flow cytometry with a Miltenyi flow cytometer.

Clonogenic Assay

Quantification of colony formation was performed according to standard protocols. See Supplemental Experimental Procedures for a detailed description.

Cytogenetic Analysis

The dose of 2 Gy was chosen to allow cells to enter mitosis after irradiation. Five hours after irradiation the cells were arrested in mitosis for 1 hr 45 min. Chromosomes were harvested, DNA stained, and telomeres detected by fluorescence in situ hybridization according to standard protocols. A detailed description is provided in Supplemental Experimental Procedures.

Statistical Analysis

Statistical analysis was performed using the two-sided Student's t test except for the comet assay, which was analyzed using ANOVA. p Values of <0.05 were considered statistically significant, with $p < 0.01$ highly statistically significant. Error bars represent the SD of the mean.

Cell culture, neutral comet assay, immunoblot analysis, immunocytochemistry, and immunohistochemistry on adult WT mouse tissue were performed using standard protocols. For a detailed description as well as antibody information, see Supplemental Experimental Procedures.

Procedures for all experiments involving animals were approved by the Animal Studies Committee at Washington University Medical Center.

SUPPLEMENTAL INFORMATION

Supplemental Information includes Supplemental Experimental Procedures and four figures and can be found with this article online at http://dx.doi.org/10.1016/j.stemcr.2016.11.004.

AUTHOR CONTRIBUTIONS

G.G.S. conceived the project. G.G.S. and B.M. designed the experiments. B.M., M.R.F., S.R., and C.L.Z performed the experiments. D.E.H. and G.G.S. helped with inputs and interpretation of the data. B.M. and G.G.S. wrote the paper.

ACKNOWLEDGMENTS

We thank Dr. Mariana Beltcheva of the human stem cell core facility for technical support in human stem cell culture, and Dr. Leonard Guarente for providing the SIRT6-GFP-plasmid. Funding was provided by NIH-R01CA174966; Department of Radiation Oncology and the Siteman Cancer Center of Washington University School of Medicine.

Received: July 19, 2016
Revised: November 7, 2016
Accepted: November 8, 2016
Published: December 13, 2016

REFERENCES

Ayrapetov, M.K., Gursoy-Yuzugullu, O., Xu, C., Xu, Y., and Price, B.D. (2014). DNA double-strand breaks promote methylation of histone H3 on lysine 9 and transient formation of repressive chromatin. Proc. Natl. Acad. Sci. USA *111*, 9169–9174.

Azuara, V., Perry, P., Sauer, S., Spivakov, M., Jørgensen, H.F., John, R.M., Gouti, M., Casanova, M., Warnes, G., Merkenschlager, M., et al. (2006). Chromatin signatures of pluripotent cell lines. Nat. Cell Biol. *8*, 532–538.

Bártová, E., Šustáčková, G., Stixová, L., Kozubek, S., Legartová, S., and Foltánková, V. (2011). Recruitment of Oct4 protein to UV-damaged chromatin in embryonic stem cells. PLoS One *6*, e27281.

Burgess, R.C., Burman, B., Kruhlak, M.J., and Misteli, T. (2014). Activation of DNA damage response signaling by condensed chromatin. Cell Rep. *9*, 1703–1717.

Chen, T., and Dent, S.Y.R. (2014). Chromatin modifiers and remodellers: regulators of cellular differentiation. Nat. Rev. Genet. *15*, 93–106.

Grewal, S.I.S., and Jia, S. (2007). Heterochromatin revisited. Nat. Rev. Genet. *8*, 35–46.

Hong, Y., and Stambrook, P.J. (2004). Restoration of an absent G1 arrest and protection from apoptosis in embryonic stem cells after ionizing radiation. Proc. Natl. Acad. Sci. USA *101*, 14443–14448.

Jacobs, K.M., Misri, S., Meyer, B., Raj, S., Zobel, C.L., Sleckman, B.P., Hallahan, D.E., and Sharma, G.G. (2016). Unique epigenetic influence of H2AX phosphorylation and H3K56 acetylation on normal stem cell radioresponses. Mol. Biol. Cell *27*, 1332–1345.

Lee, J.-H., Hart, S.R.L., and Skalnik, D.G. (2004). Histone deacetylase activity is required for embryonic stem cell differentiation. Genesis *38*, 32–38.

Lemaître, C., and Soutoglou, E. (2014). Double strand break (DSB) repair in heterochromatin and heterochromatin proteins in DSB repair. DNA Repair (Amst.) *19*, 163–168.

Loh, Y.H., Zhang, W., Chen, X., George, J., and Ng, H.H. (2007). Jmjd1a and Jmjd2c histone H3 Lys 9 demethylases regulate self-renewal in embryonic stem cells. Genes Dev. *21*, 2545–2557.

Meshorer, E., Yellajoshula, D., George, E., Scambler, P.J., Brown, D.T., and Misteli, T. (2006). Hyperdynamic plasticity of chromatin proteins in pluripotent embryonic stem cells. Dev. Cell *10*, 105–116.

Oberdoerffer, P., Michan, S., McVay, M., Mostoslavsky, R., Vann, J., Park, S.K., Hartlerode, A., Stegmuller, J., Hafner, A., Loerch, P., et al. (2008). SIRT1 redistribution on chromatin promotes genomic stability but alters gene expression during aging. Cell *135*, 907–918.

Perez-Campo, F.M., Costa, G., Lie-A-Ling, M., Stifani, S., Kouskoff, V., and Lacaud, G. (2014). MOZ-mediated repression of p16INK4a is critical for the self-renewal of neural and hematopoietic stem cells. Stem Cells *32*, 1591–1601.

Price, B.D., and D'Andrea, A.D. (2013). Chromatin remodeling at DNA double-strand breaks. Cell *152*, 1344–1354.

Robles, V., Marti, M., and Izpisua Belmonte, J.C. (2011). Study of pluripotency markers in zebrafish embryos and transient embryonic stem cell cultures. Zebrafish *8*, 57–63.

Rokudai, S., Aikawa, Y., Tagata, Y., Tsuchida, N., Taya, Y., and Kitabayashi, I. (2009). Monocytic leukemia zinc finger (MOZ) interacts with p53 to induce p21 expression and cell-cycle arrest. J. Biol. Chem. *284*, 237–244.

Sheikh, B.N., Phipson, B., El-Saafin, F., Vanyai, H.K., Downer, N.L., Bird, M.J., Kueh, A.J., May, R.E., Smyth, G.K., Voss, A.K., and Thomas, T. (2015a). MOZ (MYST3, KAT6A) inhibits senescence via the INK4A-ARF pathway. Oncogene *34*, 5807–5820.

Sheikh, B.N., Lee, S.C., El-Saafin, F., Vanyai, H.K., Hu, Y., Pang, S.H., Grabow, S., Strasser, A., Nutt, S.L., Alexander, W.S., et al. (2015b). MOZ regulates B-cell progenitors and, consequently, Moz haploinsufficiency dramatically retards MYC-induced lymphoma development. Blood *125*, 1910–1921.

Shiloh, Y., and Ziv, Y. (2013). The ATM protein kinase: regulating the cellular response to genotoxic stress, and more. Nat. Rev. Mol. Cell Biol. *14*, 197–210.

Song, N., Liu, J., An, S., Nishino, T., Hishikawa, Y., and Koji, T. (2011). Immunohistochemical analysis of histone H3 modifications in germ cells during mouse spermatogenesis. Acta Histochem. Cytochem. *44*, 183–190.

Sun, Y., Xu, Y., Roy, K., and Price, B.D. (2007). DNA damage-induced acetylation of lysine 3016 of ATM activates ATM kinase activity. Mol. Cell. Biol. *27*, 8502–8509.

Sun, Y., Jiang, X., Xu, Y., Ayrapetov, M.K., Moreau, L.A., Whetstine, J.R., and Price, B.D. (2009). Histone H3 methylation links DNA damage detection to activation of the tumour suppressor Tip60. Nat. Cell Biol. *11*, 1376–1382.

Voss, A.K., Collin, C., Dixon, M.P., and Thomas, T. (2009). Moz and retinoic acid coordinately regulate H3K9 acetylation, Hox gene expression, and Segment Identity. Dev. Cell *17*, 674–686.

Wu, X., Northcott, P.A., Dubuc, A., Dupuy, A.J., Shih, D.J.H., Witt, H., Croul, S., Bouffet, E., Fults, D.W., Eberhart, C.G., et al. (2012). Clonal selection drives genetic divergence of metastatic medulloblastoma. Nature *482*, 529–533.

Stem Cell Reports, Volume *7*

Supplemental Information

Histone H3 Lysine 9 Acetylation Obstructs ATM Activation and Promotes Ionizing Radiation Sensitivity in Normal Stem Cells

Barbara Meyer, Maria Rita Fabbrizi, Suyash Raj, Cheri L. Zobel, Dennis E. Hallahan, and Girdhar G. Sharma

Figure S1, related to Figure 1

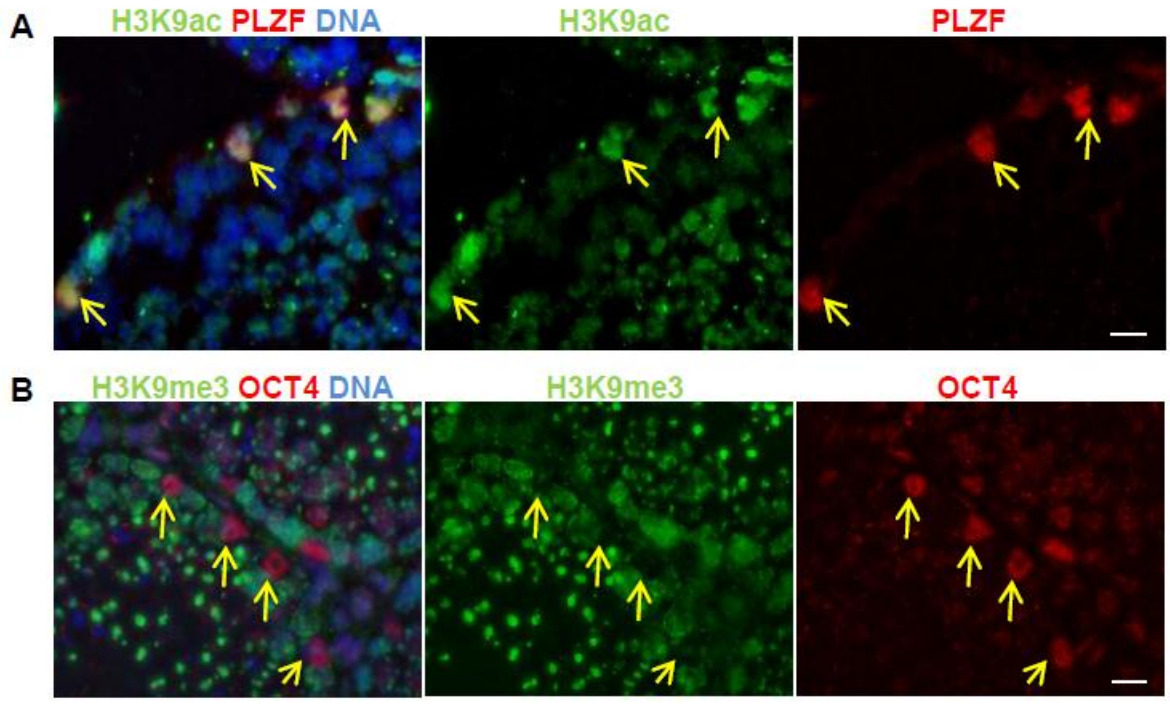

Figure S1, related to Figure 1

(A) H3K9ac, stem cell marker PLZF (promyelocytic leukemia zinc finger protein) and the DNA by DAPI staining were detected in tissue sections of adult murine testis.

(B) H3K9me3, stem cell marker OCT4 and the DNA by DAPI staining were detected in tissue sections of adult murine testis.

Arrows indicate spermatogonial stem cells. Scale bar = 10 μm.

Figure S2, related to Figure 2

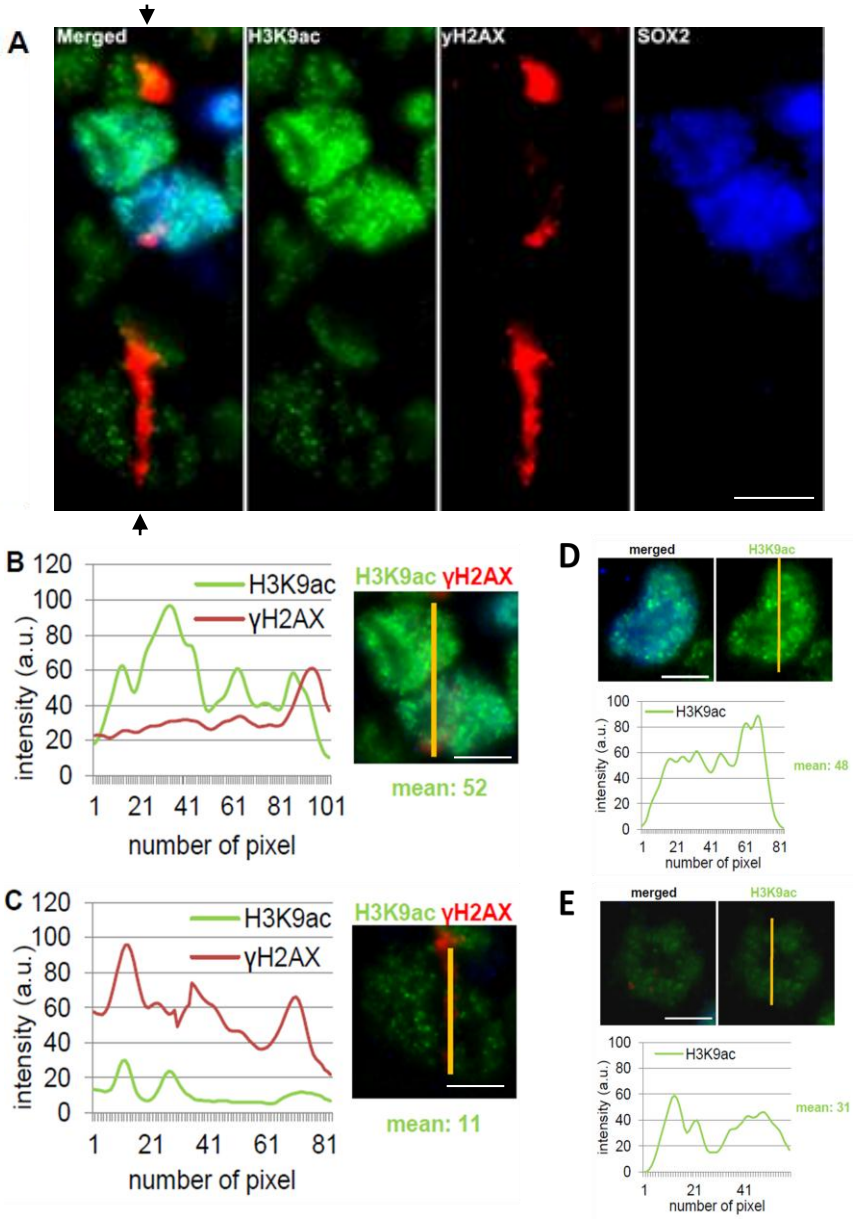

F	H3K9ac					
	< 2 mins		< 5 mins		> 5 mins	
	Deacetylated	Unchanged	Deacetylated	Unchanged	Deacetylated	Unchanged
ES (n=40)	40%	60%	40%	60%	40%	60%
ED (n=45)	80%	20%	90%	10%	90%	10%
	H3K9me3					
	< 2 mins		< 5 mins		> 5 mins	
	Methylated	Unchanged	Methylated	Unchanged	Methylated	Unchanged
ES (n=30)	5%	95%	5%	95%	5%	95%
ED (n=30)	90%	10%	40%	60%	5%	95%

Figure S2, related to Figure 2

(A) Uncropped image showing stem (ES) and non-stem (ED) cells (cropped pictures shown in Figure 2). ES and ED cells were co-plated, micro-irradiated and after fixation H3K9ac, γH2AX and SOX2 detected. Black arrows on top and bottom of the merged colors image indicate the line of micro-irradiation through ES and ED cells.

(B) Intensity profile of H3K9ac and γH2AX along the yellow line of ES cells as Figure 2SA.

(C) Intensity profile of H3K9ac and γH2AX along the yellow line of ED cells as Figure 2SA.

(D) Unirradiated ES cell was fixed and H3K9ac, γH2AX and SOX2 detected. All markers are shown in the merged image (upper left) or H3K9ac alone (upper right). Lower image shows intensity profile of H3K9ac along the yellow line.

(E) Unirradiated ED cell treated as in (D). Lower image shows intensity profile of H3K9ac along the yellow line.

(F) The percentage of ES and ED cells showing a deacetylation of H3K9ac or no change in H3K9ac at DNA damage sites after laser irradiation as well as cells showing a trimethylation of H3K9 or no change was quantified at different time endopoints. N= number of analyzed cells, pooled from at least 3 independent experiments.

In the line profiles shown in (B), (C), (D) and (E) for every depicted intensity value an average of 5 adjacent pixel was calculated.

Mean = mean intensity value of H3K9ac from all values of the line profile. Scale bars = 10 µm.

Figure S3, related to Figure 3

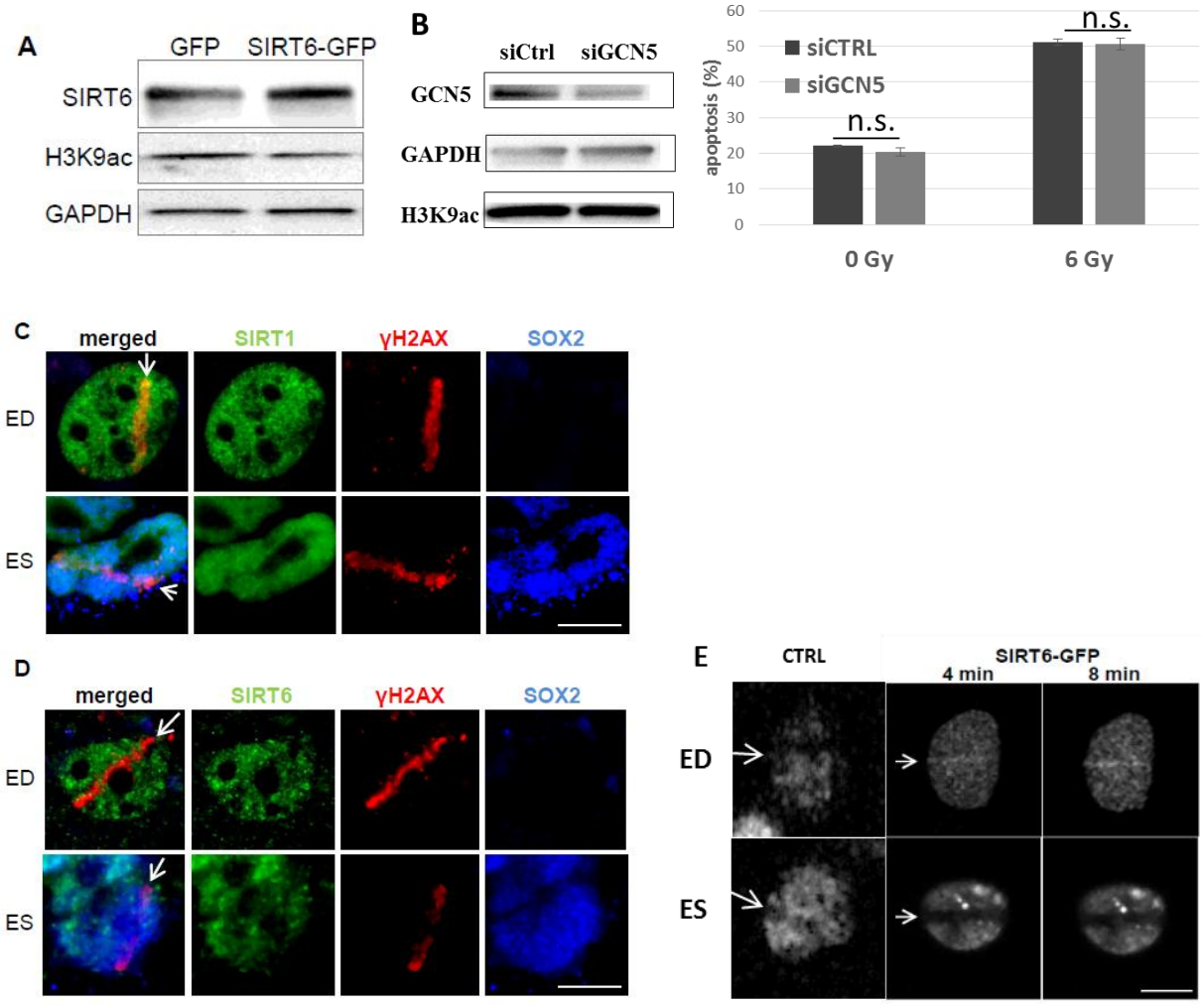

Figure S3, related to figure3

(A) Embryonic stem cells were transfected with GFP-plasmid or SIRT6-GFP-plasmid and SIRT6, H3K9ac and GADPH detected at 24h after transfection by immunoblot.

(B) Embryonic stem cells were treated with siCTRL and GCN5 siRNA: H3K9ac and GADPH detected by immunoblot (left) and apoptosis analyzed 16 h after irradiation by Annexin V labeling (right). 3 independent experiments performed.

(C) ES and ED cells were micro-irradiated, fixed and SIRT1, γH2AX and SOX2 detected.

(D) ES and ED cells were micro-irradiated, fixed and SIRT6, γH2AX and SOX2 detected.

(E) ED cell (upper panel) and ES cell (lower panel) transfected with GFP-plasmid (CTRL) and SIRT6-GFP were micro-irradiated and SIRT6-GFP detected at 4 and 8 min after irradiation.

White arrows indicate direction of laser irradiation. Scale bar = 10 µm.

Error bars = SD; n.s. = p>0.05.

Figure S4, related to Figure 4

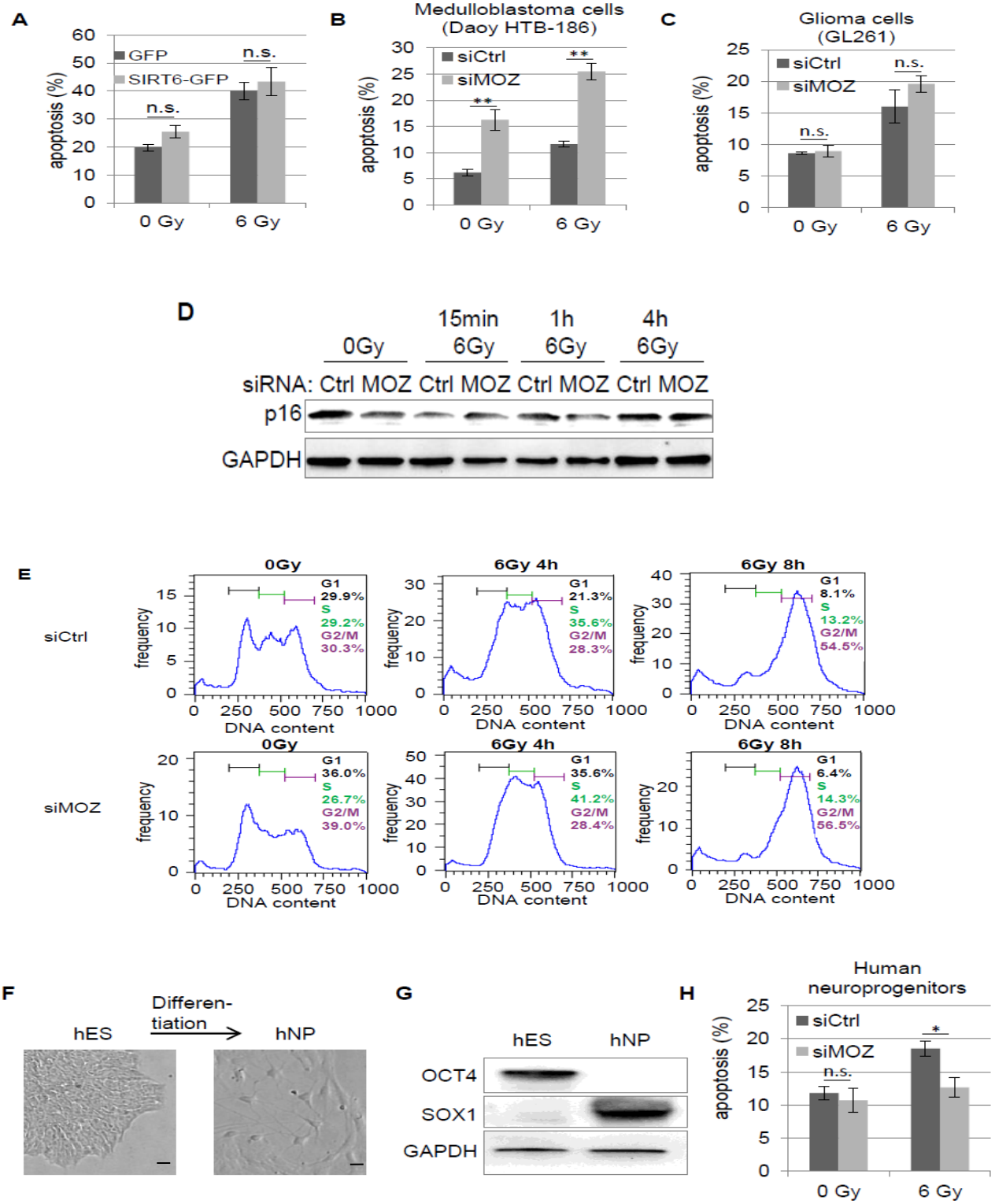

Figure S4, Related to Figure 4

(A) Embryonic stem cells were transfected with GFP-plasmid or SIRT6-GFP-plasmid, irradiated 24 h after transfection and apoptosis analyzed 16 h after irradiation by Annexin V labeling. 3 independent experiments performed.
(B) Human medulloblastoma cells (Daoy HTB-186) treated with control (siCtrl) or MOZ siRNA (siMOZ) were irradiated and apoptosis quantified at 16 h by Annexin V labeling. 3 independent experiments performed.
(C) Same assay and treatment as (B), but murine glioblastoma cells (GL261) were analyzed. 3 independent experiments performed.
(D) p16 and GAPDH were detected by immunoblot using lysates of murine ES cells treated with siRNA as in (B) and harvested at indicated timepoints.
(E) Murine ES cells were treated with siRNA as in (B) were harvested at indicated timepoints and DNA content analyzed by propidium iodide (PI) staining and flow cytometry.
(F) Micrographs of human ES cells (hES) and from these cells directly differentiated neuroprogenitors (hNP).
(G) OCT4, SOX1 and GAPDH levels of cells as in (F) were detected in the immunoblot.
(H) Human neuroprogenitors were treated with siRNA as in (B) and apoptosis analyzed 24 h after irradiation by Annexin V labeling. 3 independent experiments performed.
Error bars = SD; * = $p<0.05$; ** = $p<0.01$; n.s. = $p>0.05$. Scale bar = 10 µm.

SUPPLEMENTAL EXPERIMENTAL PROCEDURES

Cell culture and undirected differentiation

Wild-type murine embryonic stem cells (LK-1 used throughout this study, EDJ22 were used only as comparison to LK-1 cells in Figure 4B) were originally isolated from mouse blastocysts and obtained from the Murine Embryonic Stem Cell Core at Washington University in Saint Louis. Cells were cultured as previously described for EDJ22 and RW.4 cells (Jacobs et al., 2016). Cells were karyotypical normal and cultured for not more than 20 passages and tested bi-monthly for mycoplasma. Undirected differentiation of cells was achieved by depletion of LIF (leukemia inhibitory factor) and beta-mercaptoethanol for at least 4 days as described earlier (Jacobs et al., 2016). Human medulloblastoma cells (Daoy HTB-186, obtained from ATCC) were cultured in MEM containing 10 % serum and murine glioma cells GL261 were obtained from the National Cancer Institute and cultured in DMEM/F12 containing 10 % serum. Neural stem cells were isolated from the dentate gyrus of P0-P2 newborn mice and cultured or differentiated. After dissection of the hippocampal region, cells were dissociated by pipetting the tissue up and down and neural stem cells were cultured in suspension in dishes non-treated for tissue culture. Neural stem cells were cultured in AB2 Basal Neural Medium (Aruna Biomedical) containing 20 ng/ml EGF (epidermal growth factor), 10 ng/ml bFGF (basic fibroblast growth factor), 1 % N2-Supplement and 2 % B27 (Invitrogen). Differentiation of neural stem cells was induced by culturing cells for at least 5 days with 10 % serum (Hyclone) and without EGF/FGF on tissue culture-treated dishes for attachment.
Human neuroprogenitor cells were cultured at the Human Embryonic Stem Cell core facility of Washington University. We directly derived the cells from H9 cells grown on Matrigel covered plates in mTeSRTM1 with supplement (Stem Cell Technologies) and passaged using ReLeSRTM (Stem Cell Technologies) and 5 μM Rock inhibitor (Calbiochem). They were differentiated into the neural lineage using the Stem Cell Technologies monolayer protocol. For this, cells were grown on poly-L-ornithine and laminin coated plates for several days in STEMdiffTM Neural Induction Medium and several days in STEMdiffTM Neural Progenitor Medium containing supplement A and B, using accutase for passages.

X-ray irradiation and microirradiation

Cells were irradiated with 160 keV X-rays with indicated doses at a dose rate of 1.7 Gy/min in an RS-2000 Biological Research Irradiatior (Rad-Source). For microirradiation co-plated embryonic and differentiated cells were cultured for 2 days in 70 μM BrdU and irradiated with a 405 nm and 633 nm laser using a LSM 510 Confocal Microscope (Zeiss, Plan-APOCHROMAT 63x/1.4 oil objective) with incubation chamber as previously described (Jacobs et al., 2016). Stem cells were identified directly before irradiation by CDy1 (Active Motif) according to manufacturer's instructions in order to target stem cells growing adjacent to differentiated cells. ZEN software was used to select cells and target irradiation. Fixation of cells for immunofluorescence staining was performed immediately after irradiation.

RNA interference

24 h after plating cells were transfected using RNAiMAX Lipofectamine (Invitrogen) according to the manufacturer's instructions. siRNA against murine or human MOZ (Santa Cruz, sc-149523 mouse, sc-37959 human), GCN5 (Santa Cruiz, sc-37947) and Suv39h1 (Santa Cruz, sc-38464 mouse) was used at an end concentration of 50 nM and incubated 24 h before irradiation. According to manufacturer, siRNA products consist of pools of three to five target-specific 19-25 nt siRNAs designed to specifically knockdown gene expression. As control cells were transfected with the same concentration of non-targeted control siRNA (Dharmacon).

Plasmid transfection

SIRT6-GFP-plasmid (Liszt et al., 2005) was obtained from Addgene (#20275) and to generate control GFP-plasmid the SIRT6 insert was cut out using BamHI and BglII (New England Biolabs). Efficient restriction digest was tested by gel electrophoresis. For transfection of plasmids Lipofectamine LTX with Plus Reagent (Invitrogen) was used according to manufacturer's instructions. Transfection efficiency (80 % for GFP-plasmid, 55% for Sirt6-GFP-plasmid) was evaluated 24 h after transfection by measuring GFP positivity using flow cytometry. Only GFP-positive cells were analyzed for apoptosis induction.

Inhibitors

ATM inhibitor (Sigma Aldrich, KU-55933) was dissolved in DMSO and the cells incubated with 10 µM inhibitor for 1h prior irradiation.

Immunoblot

Trypsinized cells were lysed in RIPA buffer (Thermo Scientific) containing protease inhibitor cocktail, 1 mM PMSF and phosphatase inhibitors (Sigma). Lysates were sonicated in 5 times for 30 seconds, centrifuged for 15 min at 8000 g and protein concentration determined using the BCA protein assay (Thermo Scientific). 15 µg of lysate were loaded on a 4 - 15 % tris glycine PAA-Gel (BioRad) using tris glycine running buffer (novex). Protein size was determined with the Kaleidoscope prestained marker (BioRad). Transfer to a PVDF membrane was performed in a wet chamber with tris glycine transfer buffer (novex). For blocking the membrane was incubated in 5 % milk or BSA in TBS-T for 30 min. Primary antibodies against phospho-S1981-ATM (Cell Signaling, 10H11.E12, mouse, 1:1000 in milk), MOZ (Acris, AP00341PU-N, rabbit, 1:200 in BSA), Suv39h1 (Abgent, rabbit, 1:500 in milk), SIRT6 (Proteintech Group, 13572-1-AP, rabbit, 1:1000 in BSA) GAPDH (Sigma Aldrich, G8795, mouse, 1:100,000 in milk), H3K9ac (Millipore, 06-942, rabbit, 1:1000 in BSA), H3K9me3 (Millipore, CMA308, mouse, 1:25,000 in BSA), SOX2 (Abcam, ab79351, mouse, 1:1000 in BSA), SOX1 (R&D Systems, AF3369 , goat, 1:1000 in BSA), OCT4 (Abcam, ab19857, rabbit, 1:1000 in BSA), p16 (Thermo Scientific, MA5-17142, mouse, 1:5000 in BSA) were incubated over night at 4 ◦C and secondary peroxidase conjugated antibodies (anti mouse or anti rabbit, Sigma, 1:5000; anti goat Santa Cruz 1:5000) for 2 h at RT. The chemoluminescence signal was detected with ECL substrate (GE/Pierce) in a ChemiDoc MP digital system (BioRad).

Cell cycle measurement

Cells were harvested using trypsin, washed with PBS and resuspended in 500 µl cold PBS. 2 ml of cold 100% EtOH were added drop-wise while vortexing cells slowly. Samples were stored at -20◦C until staining. After centrifugation for 8 min at 1800 g, PBS wash and centrifugation at 500 for 8 min, cells were incubated in 100 µl 0.1 µg/µl RNase (Cell Signaling) in PBS for 1h 15 min at 37◦C. 200 µl 1 µg/µl propidium iodide (BD Pharmingen) in PBS were added and samples incubated 10 min at RT until measurement with flow cytometer.

Immunofluorescence staining

For analysis with flow cytometry cells were trypsinized, washed with PBS, fixed 5 min with 4 % formaldehyde in PBS, permeabilized 2 min in 0.2 % Triton X-100 in PBS, washed with PBS and blocked in 2 % BSA in PBS over night at 4 ◦C. Centrifugation steps were carried out at 300 g before fixation and 800 g after fixation for at least 5 min. Cells were incubated with antibodies against phospho-S1981-ATM (Cell Signaling, 10H11.E12, mouse, 1:200) diluted in 2% BSA/PBS for 1 h at RT. After washing in PBS cells were incubated with anti-mouse FITC antibody (Vectashield, 1:100) for 1 h at RT. After washing in PBS signal intensities of 1000 cells were measured using a Miltenyi flow cytometer.

For microscopy cells were grown on cover slips and fixed for 5 min with 4 % formaldehyde in PBS and permeabilized for 4 min in 0.2 % Triton X-100 in PBS. After several washes in PBS, samples were incubated at least 20 min with 2 % BSA in PBS. Incubation with primary or secondary antibody was conducted for 1 h at 37◦C. For antibody staining of microscopy samples standard protocols were used as described earlier (Jacobs et al., 2016). The following primary antibodies were used: H3K9ac (Millipore, 06-942, rabbit 1:200), H3K9me3 (Millipore, CMA308, mouse, 1:200), γH2AX (Millipore, 05-636, mouse, 1:1000), SIRT1 (Millipore, 07-131, rabbit, 1:200), SIRT6 (Proteintech, 13572-1-AP, rabbit, 1:100), SOX2 (Abcam, ab79351, mouse, 1:200) and OCT4 (Abcam, ab19857, rabbit, 1:200). Secondary anti-rabbit and anti-mouse antibodies conjugated to fluorescein, Texas Red or AMCA (Vector) were used at a dilution of 1:100. Samples were mounted in Vectashield mounting medium containing DAPI (Vector).

Three-color staining of micro-irradiation samples required a sequential staining as described previously (Jacobs et al., 2016). For this, samples were incubated with anti-H3K9ac (rabbit), anti-SOX2 (mouse) and secondary antibody dilutions (anti-mouse-AMCA and anti-rabbit-fluorescein) as described above. This was followed by a 5 min incubation with γH2AX antibody dilution and subsequent 5 min incubation with anti-mouse Texas Red-conjugated antibody. Short 5 min incubation times were chosen to avoid cross reactivity between anti-mouse antibody stainings.

Samples showing nuclear-wide binding of anti-mouse-Texas Red antibody to Sox2 antibody were excluded from evaluation.

Immunhistochemistry

6-8 weeks old male C57BL/6 mice were sacrificed and tissues frozen in OCT media. Cryosections of 10 µm thickness were obtained from the histology core at Washington University. Frozen sections were thawed in cold PBS, fixed for 15 min in 4 % formaldehyde in PBS and permeabilized in 0.2 % Triton-X-100 in PBS for 15 min. After several short PBS washes sections were blocked in 2 % BSA in PBS for 1 h. Antibodies against H3K9ac (Millipore, 06-942, rabbit, 1:200), H3K9me3 (Millipore, CMA308, mouse, 1:200), H3K9me3 (Abcam, ab8898, mouse, 1:1000) together with SOX2 (Abcam, ab79351, mouse, 1:100), PLZF (Santa Cruz, sc-28319, mouse, 1:50), OCT4 (Abcam, ab19857, rabbit, 1:200) or H3 (Cell Signaling, D1H2, rabbit, 1:250) were used for 2 h in a wet chamber at 37 ◦C. After PBS washes secondary antibody (1:100, Vector) incubation was carried out for 45 min. Slides were washed, dried and mounted in Vectashield mounting medium containing DAPI (Vector).

Microscopy and image processing

Imaging was performed using a Zeiss Axioplan 2 microscope with 20x, 63x or 100x objectives (Plan-NEOFLUAR 20x/0.5, Plan-APOCHROMAT 63x/1.4 Oil, Plan-NEOFLUAR 100x/1.3 Oil) and Meta Systems ISIS imaging software. ImageJ was used to process micrographs, which included cropping of images and minimal adjustment of signal intensity. All images of one experiment were processed in the same way.

Neutral Comet Assay

At indicated timepoints after irradiation cells were trypsinized, centrifuged for 5 min at 300 g and resuspended in media to a final concentration of $0.5*10^6$ cells/ml. 5 µl of this cell suspension were resuspended in 50 µl prewarmed (37◦C) agarose (Trevigen) and distributed on a glass slide (CometSlide, Trevigen). Slides were cooled at 4◦C for 15 min and incubated in lysis solution (Trevigen) at 4◦C for 1h. After lysis slides were shortly washed in water and stored in cold TAE. After collection of all samples electrophoresis was conducted in a cooled chamber (Hoefer Scientific instruments) with TAE at 25 V for 35 min. Slides were washed in water, dried and stained with SybrGreen (Trevigen) for 90 min. After additional washes in water slides were dried. Images were taken using a Zeiss Axioplan 2 microscope using a 20x objective. Evaluation of olive moments was performed with CometScore software (TriTek).

Clonogenic assay

LK-1 murine embryonic stem cells with 24 h of MOZ siRNA treatment were irradiated with indicated doses and incubated 6 h after irradiation to allow for DNA repair to occur. Cells were then trypsinized and counted using a Vi-Cell cell counter. The same number of cells for control and MOZ siRNA treated cells were plated and grown for 7 days. Fixation was performed by PBS wash and incubation in cold methanol on ice for 10 min. For staining cells were incubated for 10 min with crystal violet (Sigma) at RT. Cells were washed twice with water, dried and counted. Plating efficiency for LK-1 cells was 15 %.

Cytogenetic analysis

24 h after MOZ or control siRNA treatment cells were irradiated. The dose of 2 Gy was chosen to still allow cells to enter mitosis after irradiation. 5 h after irradiation cells were treated with 100 ng/ml colcemid (Gibco) for additional 1 h and 45 min. Mitotic shake-off in cold trypsin was performed, harvested cells were centrifuged for 8 min at 250 g and treated with hypotonic buffer (0.56 % KCl) for 8 min. Samples were fixed in acetic acid/methanol (1:3) for at least 45 min and fluorescence-*in-situ*-hybridization of telomeres performed as previously described (Jacobs et al., 2016). Stained chromosomes were mounted in Vectashield mounting medium containing DAPI (Vector). Imaging of chromosomes was performed using Zeiss Axioplan 2 microscope with a 20 x objective. Chromosome aberrations were defined as chromosome or chromatid breaks, translocations or radials. At least 40 chromosome plates were scored.

SUPPLEMENTAL REFERENCE

Liszt, G., Ford, E., Kurtev, M., and Guarente, L. (2005). Mouse Sir2 homolog SIRT6 is a nuclear ADP-ribosyltransferase. J. Biol. Chem. *280*, 21313–21320.